A GIS-based methodology for assigning experimental measurements of angular distribution of sky radiance and luminance to selected sky sectors

Ignacio García[a,b,*], Almudena García[a,b] and José Luis Torres[a,b]

[a] Department of Engineering, Public University of Navarre, Campus Arrosadía, 31006 Pamplona, Spain.
[b] Institute of Smart Cities (ISC), Public University of Navarre, Campus Arrosadía, 31006 Pamplona, Spain.
[*] Corresponding author: Tel.: +34 948 169689, email: ignacio.garcia@unavarra.es

Abstract

Mathematical models for the estimation of the angular distribution of diffuse radiance/luminance in the sky describe the anisotropic character of diffuse solar radiation and daylight in the sky vault. In most of these models the radiance/luminance of a sky point is determined by the product of the indicatrix function and the gradation function. When developing and/or calibrating these models, it is typical to consider separately the dispersion effects in the direction of the sun's rays and the gradation from the zenith towards the horizon. To do this, the sky is divided into a number of concentric spherical zones around the sun and a number of concentric spherical zones around the zenith. The intersection between both sets of zones delimits a series of sky elements. Unfortunately, these sky elements do not correspond to the 145 patches of sky vault recommended by the International Commission on Illumination (CIE), which are routinely scanned by the existing commercial sky scanners. The identification of the sky elements, geometrically different from those observed by commercial sky scanners, and the assignation of the radiance/luminance values registered by such sky scanners are not analytically trivial tasks. A GIS-based methodology is presented in this work to undertake these goals.

Keywords

Angular distribution models; Sky radiance/luminance; GIS

Nomenclature

Z = zenith angle of a sky vault point

Z_S = zenith angle of the sun

Z_e = zenith angle of an EoSS

Z_p = zenith angle of a CIE sky patch

γ = azimuth angle of a sky vault point measured from the south

γ_S = azimuth angle of the sun

γ_e = azimuth angle of an EoSS

γ_p = azimuth angle of a CIE sky patch

γ_{tosun} = azimuth angle of a sky vault point measured from the solar meridian

χ = angle between the sun and the sky vault point

χ_{p-e} = angle between the centroid of the patch and the centroid of an EoSS

L = absolute radiance/luminance of any sky point given by its coordinates (Z,γ)

L_Z = zenith radiance/luminance

L_e = absolute radiance/luminance of an EoSS

L_p = absolute radiance/luminance of a CIE sky patch

l = radiance/luminance relative to zenith of any point given by its coordinates (Z,γ)

f = indicatrix function

φ = gradation function

SSS = spherical segment of scattering

SSG = spherical segment of gradation

EoSS = element of spherical surface

n = cloud index

1. Introduction

A precise knowledge of the angular distribution of radiance and luminance in the sky vault is required when to accurately estimate the diffuse irradiance and illuminance incident on a plane of interest. The accuracy of such calculations determines the estimation reliability of the energy produced by the active solar energy conversion devices and the efficiency of the passive uses of this energy, or that of the design of lighting systems. Because sky radiance and luminance have the same origin and their angular distributions are similar, many of the proposed angular distribution models are typically used interchangeably for the two variables. In fact, their diffuse component is a consequence of the interaction between solar radiation and the atmosphere. In complex environments, such as cities, it is also the result of the interaction of solar radiation with existing obstacles. Such a diffuse component is especially important at high latitudes, where the optical path traveled by the sun's rays is long, or at the lower floors of buildings located in highly urbanized cities. Notwithstanding, this component is also significant in other locations.

Unfortunately, there are only a small number of locations in the world where the angular distribution of radiance/luminance measurements exist. Therefore, in most cases, mathematical models of different complexity are used to estimate these values. For example, the libRadtran software package for radiative transfer calculations in the Earth's atmosphere [1] allows the estimation of the radiance of a sky element located at a given position. In regard to solving the problem in clear sky conditions, this model does not require many input variables, but the situation is greatly complicated by the presence of clouds.

The work of Kocifaj [2] is an interesting advance in the theoretical modeling of real (non-homogeneous) skies as it considers the effects that the inclusion of different cloud configurations implies. This theoretical development, which is based on the principles of radiative transfer, contemplates the first and second scattering order, cloud reflectance and the interactions between ground reflections and the atmosphere. The developed version of the software, which is available on the web, performs a spectral analysis. Though, a new version is planned that addresses broadband radiance/luminance. The model requires, as radiative transfer codes, a significant number of input variables. Particularly, those related to clouds: cloud fraction, optical thickness, reflectance, shape, size and altitude, that may not be available in most locations. This compromises the applicability of the procedure, although it should be noted that some default values are proposed. No experimental validation is presented in the paper.

In the field of engineering, it is more common to use simpler models that have evolved from those that are applicable only to certain sky types to others suitable to all sky types. Within the first group are the Moon and Spencer [3] model for overcast skies and the Kittler [4] model for clear skies. These models resulted in two International Commission on Illumination (CIE) standards [5,6]. Meanwhile, the models developed by Perraudeau [7], Matsuura and Iwata [8], Perez et al. [9], Brunger and Hooper [10], Perez et al. [11], Igawa et al. [12], Igawa [13], as well as the CIE standard general sky [14], can be applicable to all sky conditions. In this study, we will only consider the second group of models.

When obtaining the radiance/luminance $L(Z,\gamma)$ of a sky point defined by the zenith angle Z and azimuth γ (see Fig. 1), it is common for models to consider separately the dispersion of the solar radiation with respect to the direction of the sun beams and the sky brightness variation from the zenith to the horizon. These two phenomena are usually modeled by means of the indicatrix $f(\chi)$ and gradation $\varphi(Z)$ functions, respectively. As a result, the basic expression used by numerous models to calculate the radiance/luminance of a sky point is that described in Equation (1).

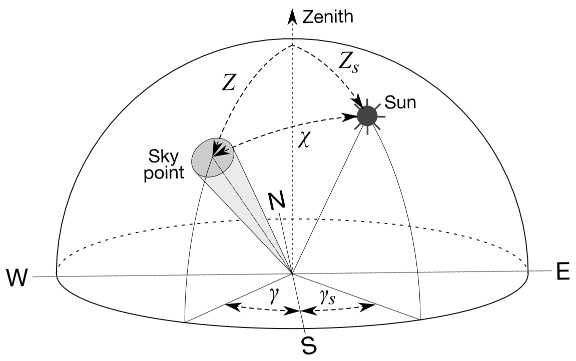

Fig. 1. Angles defining the position of the sun and a sky point.

$$L(Z,\gamma) = f(\chi)\cdot\varphi(Z) \tag{1}$$

Additionally, it is frequent to work with relative values of angular distribution, rather than absolute values. The relative radiance/luminance at a sky point $l(Z,\gamma)$ results from the ratio between its absolute radiance/luminance value and that of a reference point, as expressed in Equation (2). In this case, as usual, the reference point is the zenith.

$$l(Z,\gamma) = \frac{L(Z,\gamma)}{L_z} = \frac{L(Z,\gamma)}{L(0)} = \frac{f(\chi)\cdot\varphi(Z)}{f(Z_s)\cdot\varphi(0)} \tag{2}$$

In practice, the formulation of the indicatrix and gradation functions and their coefficients vary among the different models. Such coefficients are related to the different indicators used to characterize the sky conditions under analysis. For example, in Perez et al. [11], the gradation and indicatrix functions included two and three different coefficients, respectively. The value of these coefficients is a function of the three indicators used to characterize the sky condition, namely, the solar zenith angle, the sky brightness and the clearness index.

The indicatrix function provides the same result for all those points of the sky vault with the same angular distance to the sun (χ) at any given time and under certain sky conditions. These points result from the intersection of the sky vault with circles of increasing radius located on planes perpendicular to the direction of the solar beams (see Fig. 2.a). Meanwhile, all those points that have the same zenith angle (*Z*) and, therefore, belong to the same almucantar, have the same value of the gradation function. The almucantars were obtained from the intersection between the sky vault and circles of decreasing radius from the horizon to the zenith, located on planes parallel to the horizontal plane (see Fig. 2.b). Because an infinite number of circumferences could be considered, the spherical zones of the spherical segments between two successive circumferences concentric with the sun's rays (SSS) and the spherical zones of the spherical segments between successive almucantars (SSG) were actually used (see Fig. 2).

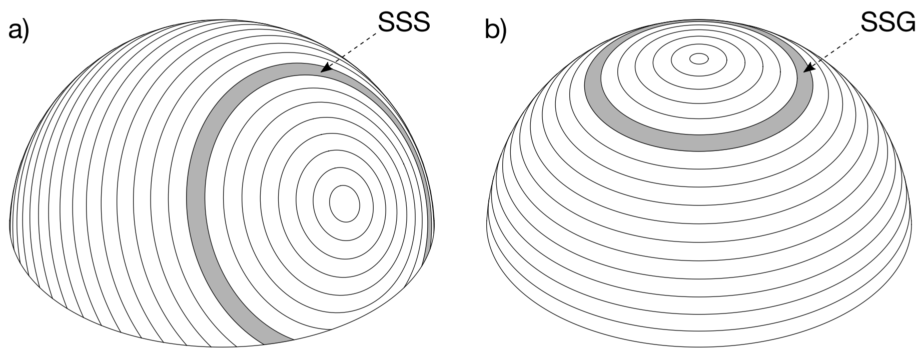

Fig. 2. Circles concentric to the sun's rays on which the indicatrix function remains constant for a Z_s of 55° (a), and circles concentric with the zenith direction (almucantars) on which the gradation function remains constant (b). A spherical segment is generated between any two circles of (a) and (b).

The size of the SSSs or SSGs will depend on the angular amplitude chosen in each case (e.g., 5º in Fig. 2). The intersection of a given SSS and a given SSG delimits an element of spherical surface (EoSS) with a shape and size dependent on the SSS and SSG considered. Some examples can be seen in the shaded areas of Fig. 3.

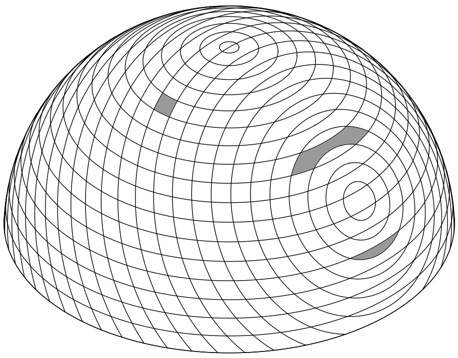

Fig. 3. Spherical surface elements (EoSS) obtained as a result of the intersection between different SSSs and SSGs.

The measurement of angular distribution of diffuse radiance and/or luminance in the sky vault is usually carried out by so-called sky scanners. On some occasions, these devices are prototypes built to be used in specific studies, as is the case of the study by Perez et al. [9]. Also, in the field of experimental devices, it is worth mentioning the portable sky scanner for measuring extremely low night-sky brightness (PePSS) described by Kocifaj et al. [15]. This system, developed by Slovak Academy of Sciences and Comenius University, allows adjusting the field of view (FOV) and programming the scanning mode. However, commercial sky scanners are the most widely used. Fig. 4 shows the commercial sky scanners manufactured by EKO and PRC Krochmann. These latest devices measure the radiance/luminance corresponding to the 145 patches of sky hemisphere shown in Fig. 5, according to the CIE Guide [16].

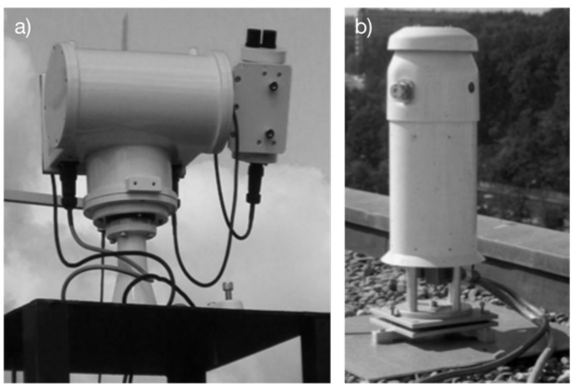

Fig. 4. Images of (a) Sky Scanner EKO, model MS-321LR, installed at Public University of Navarre and (b) Sky Scanner PRC Krochmann (photo courtesy of Dr. Pierre Ineichen).

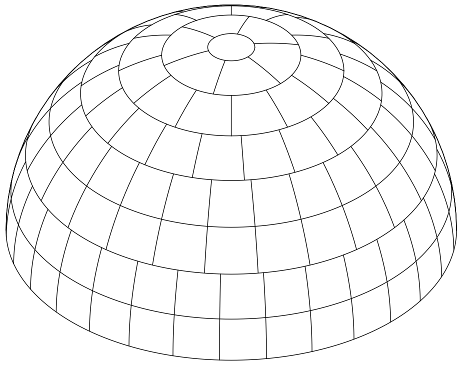

Fig. 5. Subdivision of the sky hemisphere into 145 patches according to CIE [16].

For the development and calibration of mathematical models for the estimation of the angular distribution of diffuse sky radiance/luminance, it is necessary to determine the measured values of these variables for each of the EoSS. For example, Janjai et al. [17] and Janjai [18] carried out this determination when modeling the indicatrix and gradation functions. Regarding the indicatrix function, the luminance values of the EoSSs with the same χ were determined while the luminance of the EoSSs belonging to the same almucantar was determined for the case of the gradation function. This procedure is described in the Appendix A. Given the variability of shapes of EoSSs and their dependence on the position of the sun at each moment, these sky elements do not correspond to the 145 established patches of sky vault measured by the sky scanners. Thus, to find the radiance/luminance corresponding to each EoSS at a given time, it is necessary to overlap the sky vault partition shown in Fig. 3 with that in Fig. 5. Given that an EoSS can contain portions of several sky patches, a possible approach is to assign to the EoSS the radiance/luminance resulting from the weighted mean of the radiance/luminance of the affected patches.

Unfortunately, no procedure was found in the literature for performing the two tasks previously mentioned, i.e., the delimitation of the EoSSs for each solar zenith angle and the assignation of the radiance/luminance experimental values observed in the 145 routinely registered positions of the commercial sky scanners to each of the different

EoSSs. This is not an analytically trivial procedure; thus, the objective of this work was to present a methodology that allows for the completion of the two tasks mentioned and the subsequent assignation of radiance/luminance to each EoSS using Geographical Information Systems (GIS). The purpose of this methodology is the assignment of radiance/luminance values measured by commercial sky scanners (at established sky sky positions and with a fixed FOV) to sky areas whose geometry is different from that of the sky patches observed by such sky scanners. The ultimate goal of this assignment is to model the angular distribution of radiance/luminance in the sky according to the procedure included in the Appendix A.

The procedure proposed in the next section is an easy-to-use, easily automated and versatile alternative for research in the field of angular distribution of radiance and luminance in the sky. In addition, it allows to observe the graphical evolution of the calculations, so that at any moment it is possible to visualize the patches or sectors of sky involved.

2. Methodology

A methodology based on the geometric analysis capability of GIS was developed as part of the present study. GIS tools have great potential for the analysis of geometric entities with associated numerical information.

Despite their numerous advantages, working with GIS presents two special features that condition the methodology shown below. First, the geometries corresponding to the different sky elements must be topologically correct to ensure the quality of subsequent data analyses. For example, there should be no open polygons, spaces (see Fig. 6a) or overlaps (see Fig. 6b) between adjacent polygons.

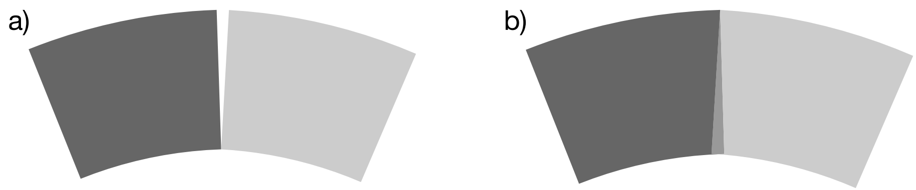

Fig. 6. Two of the most common errors in the generation of polygon geometry: holes (a) and overlaps (b).

Given the discrete nature of the sky elements used, their representations can be stored as vectors. Of all the geometric entities that the vector files can utilize to determine the variability and characteristics of the environment, the most relevant entity to the present study is the polygon since the EoSSs and sky patches are polygons.

The topology generation process involves the detection and correction of the topological errors in the initial geometric representation. Certain computer-aided design (CAD) programs and GIS allow for establishing a series of topological rules that set the spatial constraints among the elements of a plane. The elements that do not meet these constraints are highlighted by the program. In general, the intervention of a human expert is required to evaluate errors indicated by the program and implement any corrections. Topological errors are commonplace; however, a careful review of the models minimizes these errors and facilitates the topology generation process.

After the eventual geometrical correction, each polygon (EoSS or sky patch) constituted a unique graphical entity (spatial component) with associated alphanumeric information (thematic component). Thus, a unique identifier can be added to each sky element, regardless of its shape, along with a value of radiance or luminance. The generated polygons are stored in a vector file. The shapefile (SHP) vector format has been used in this work, given that its widespread use has led it to become a *de facto* standard.

The other particular feature of working in most GIS environments (especially in open source GIS) is the impossibility of applying its geoprocessing or vector analysis tools to polygons located in 3D-space. Although some GIS allow for the visualization and analysis of vector models in 3D, they do not provide geoprocessing for polygons located in 3D-space. Because only 2D-files can be used, the surfaces must be projected onto a plane. In the present study, we used equisolid projection over the horizontal plane of the sky vault. This projection preserves the solid angle of the sky spherical elements (EoSS and patches). Additionally, the spatial correspondence is maintained among the different sky segmentations. Therefore, if an EoSS covers more than one patch, it is possible to determine the solid angle proportion of the EoSS corresponding to each sky patch and calculate the radiance or luminance of this EoSS as the average of the radiance/luminance of the patches involved, proportionally weighted.

The methodology proposed encompasses six stages. The graphical results of the methodology for a Z_S of 55° can be observed in Fig. 7. For each SSG and SSS, corresponding to a solar elevation based on the establish intervals, the steps were as follows:

1. 3D-modeling of the different sky vault divisions with a CAD program. This includes the following:
   - Generate the SSSs in which the indicatrix function is constant. The geometry of these spherical segments depends on the sun's position. Thus, it is necessary to develop a model for each defined solar elevation (Fig. 7a).
   - Generate the SSGs in which the gradation function is constant in accordance with the desired angular increments of the spherical sector (Fig. 7b).
   - Generate the 145 sky patches proposed in the CIE standards (Fig. 7c).
2. Generate the orthographic projection over the horizontal plane of each model with a CAD program (Fig. 7d-Fig. 7f) to create a 2D-vector file that can be processed by GIS. The orthographic projection of the hemisphere alters the shape and area of the

geometric entities. Therefore, they should then be re-projected to an equisolid projection.

3. Generate the polygon topology for each projection along with its topological correction using a CAD program or GIS. This stage concludes with the generation of a series of shapefile files for subsequent analysis in GIS.
4. Re-project the geometric entities contained in each shapefile from orthographic to equisolid projection by means of GIS (Fig. 7g-Fig. 7i).
5. Use of the intersection geoprocessing tool provided by GIS for the graphic delimitation of the different EoSSs corresponding to each of the considered solar zenith angles. The SSG and SSS vector files generated in the previous stage act as input layers to GIS geoprocessing. The result of this operation (Fig. 7j) is a new shapefile comprising all EoSSs. Each generated EoSS also includes the alphanumeric information associated with each of the entities (SSGs and SSSs) that gave rise to the geometry.
6. Superpose the patches and EoSSs for each solar zenith angle by GIS. The intersection tool is applied again, and as in the previous case, the newly generated geometric entities (Fig. 7k) conserve the attributes of both input layers. Here, the attributes of the EoSSs and patches are conserved; thus, each of the generated polygons contains the identifier of the EoSS and the corresponding patch. In this manner, it is possible to determine the patch that corresponds to each EoSS. Furthermore, if an EoSS includes several patches, the EoSS proportion that corresponds to each patch is calculated to determine the mean weighted value of its corresponding radiance/luminance.

Once the EoSS files for the different solar elevations have been generated, as well as the shapefile corresponding to the sky scanner measurements distribution, they can be used as many times as desired. That is, for as many moments as necessary. Consequently, the steps detailed until point 5 of the procedure only have to be performed once.

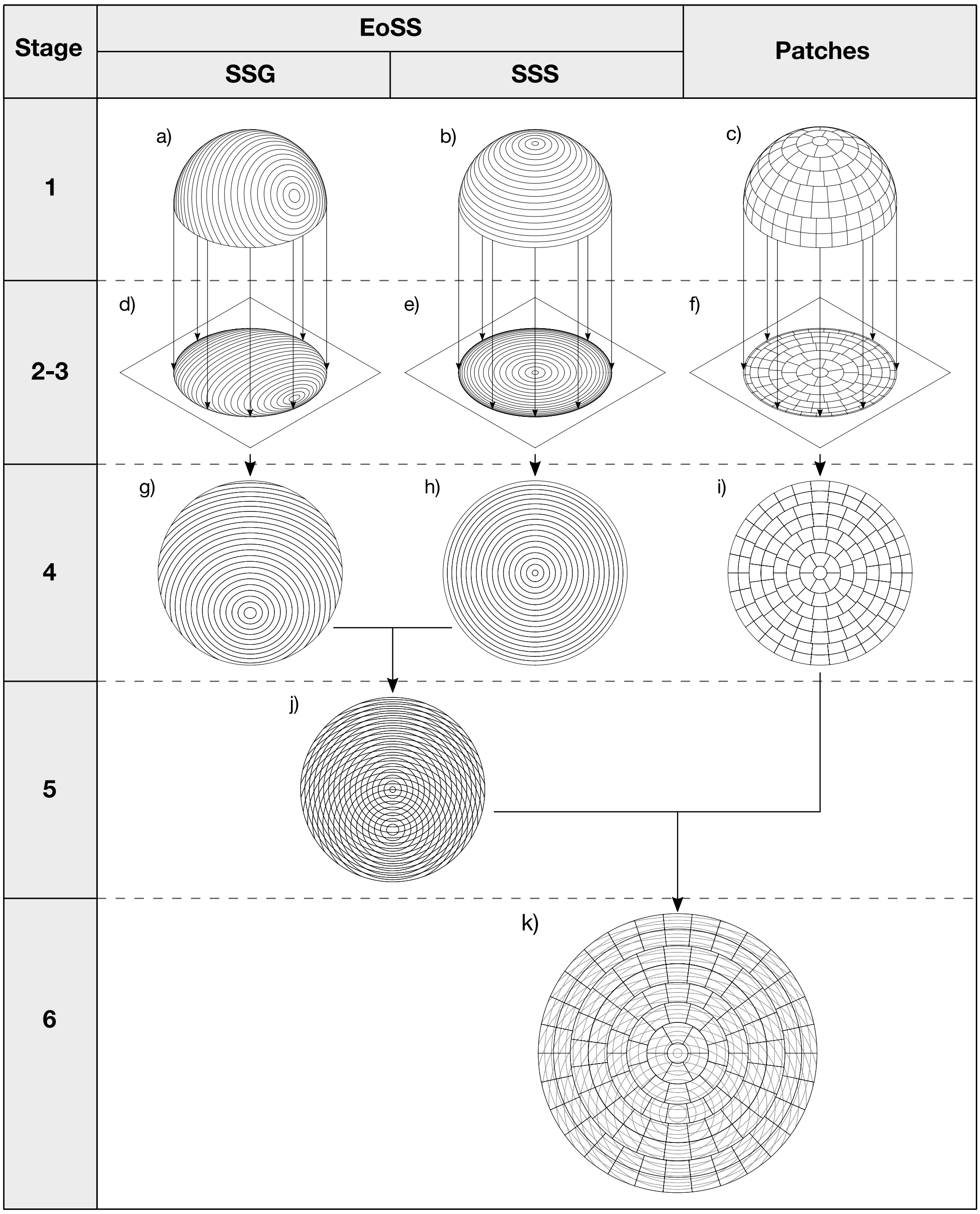

Fig. 7. Graphical representation of the methodology.

Detailed results obtained after the application of the described methodology considering a Z_S of 55° are presented in Fig. 8. Specifically, this figure shows the overlap between an EoSS and four sky patches. The luminance corresponding to the EoSS in Fig. 8 is calculated as the weighted mean of the luminance of each of the four patches, according to the proportion of the EoSS that encompasses each one.

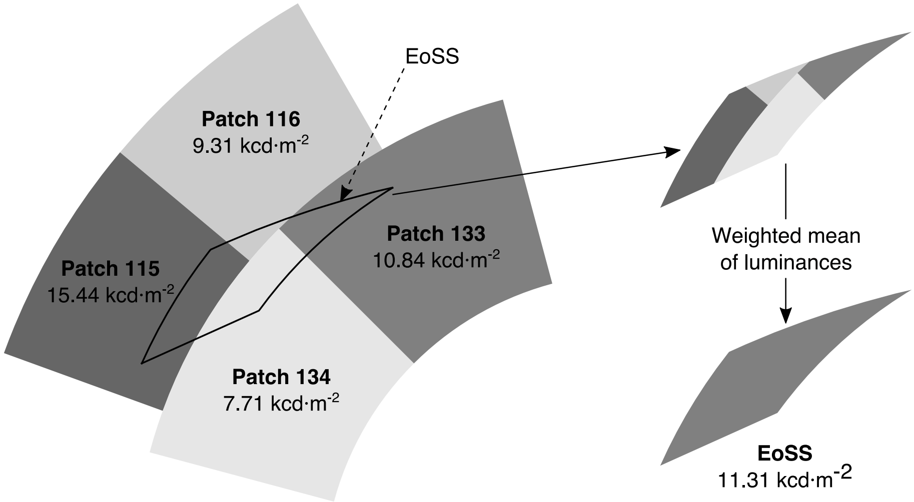

Fig. 8. Detail of an EoSS with four patches. The EoSS luminance is determined by a weighted measurement of the luminance of each patch.

3. Comparison between GIS-based method and spatial interpolation

As explained in the introduction, no conveniently detailed procedure for the assignation of the radiance/luminance experimental values measured by commercial sky scanners to of the different EoSSs has been found in the literature. However, some proposals exist for radiance/luminance determination of a certain point in the sky as the one presented by Kómar et al. [19]. In this work, the gradation and indicatrix functions from the two parts of sky vault divided by solar meridian are analyzed from the measurements of a self-constructed prototype of a portable sky scanner with calibrated spectroradiometer. For the determination of the radiance/luminance of a certain sky element defined by its zenith angle and its angular distance to the sun, a linear interpolation between four points measured by the scanner which enclose required sky element is proposed.

In order to assess the suitability of the GIS-based procedure proposed in this work it was performed a comparison between the radiance obtained by interpolation and that determined by the GIS-based procedure proposed in this paper. Thus, the inverse distance weighting (IDW) interpolation method has been applied. The application of this method requires a metric operator to consider the distance between the points of known radiance and the sky element of interest. In this case, the angular distance between the centroid of the patch and that of the EoSS ($\chi_{p\text{-}e}$), calculated according to Equation (3), has been chosen.

$$\chi_{p-e} = \arccos(\cos Z_e \cos Z_p + \sin Z_p \sin Z_e \cos|\gamma_p - \gamma_e|) \quad (3)$$

The power parameter, that controls the significance of measured radiance/luminance values on the interpolated value, was set equal to two. So, the EoSS radiance/luminance (L_e) can be determined by IDW interpolation according to Equation (4).

$$L_e = \frac{\sum_{p=1}^{4} L_p(Z_p, \gamma_p)/\chi_{p-e}^2}{\sum_{p=1}^{4} 1/\chi_{p-e}^2} \quad (4)$$

Fig. 9a shows the radiance distribution in the sky vault measured at the Public University of Navarre station (Pamplona, Spain) on 05-08-2007 at 14:00 UTC. This distribution corresponds to a standard sky type 8 according to the CIE classification [14]. This is the most frequent intermediate sky type in Pamplona, as shown in Torres et al. [20,21]. The measurements represented in Fig. 9 have been rotated to refer them to the solar meridian. The black lines superimposed on the patches represent the EoSS distribution corresponding to a solar zenith angle of 35º.

Meanwhile, Figs. 9b to 9e correspond to the four EoSS, shaded in Fig. 9a, that have been taken as example. The colored sky patches in each figure are the four closest to the EoSS, i.e. those with the smallest angular distance to the centroid of the EoSS that will be used for the interpolation cited above. Patch centroids have been marked with a black dot in the different figures.

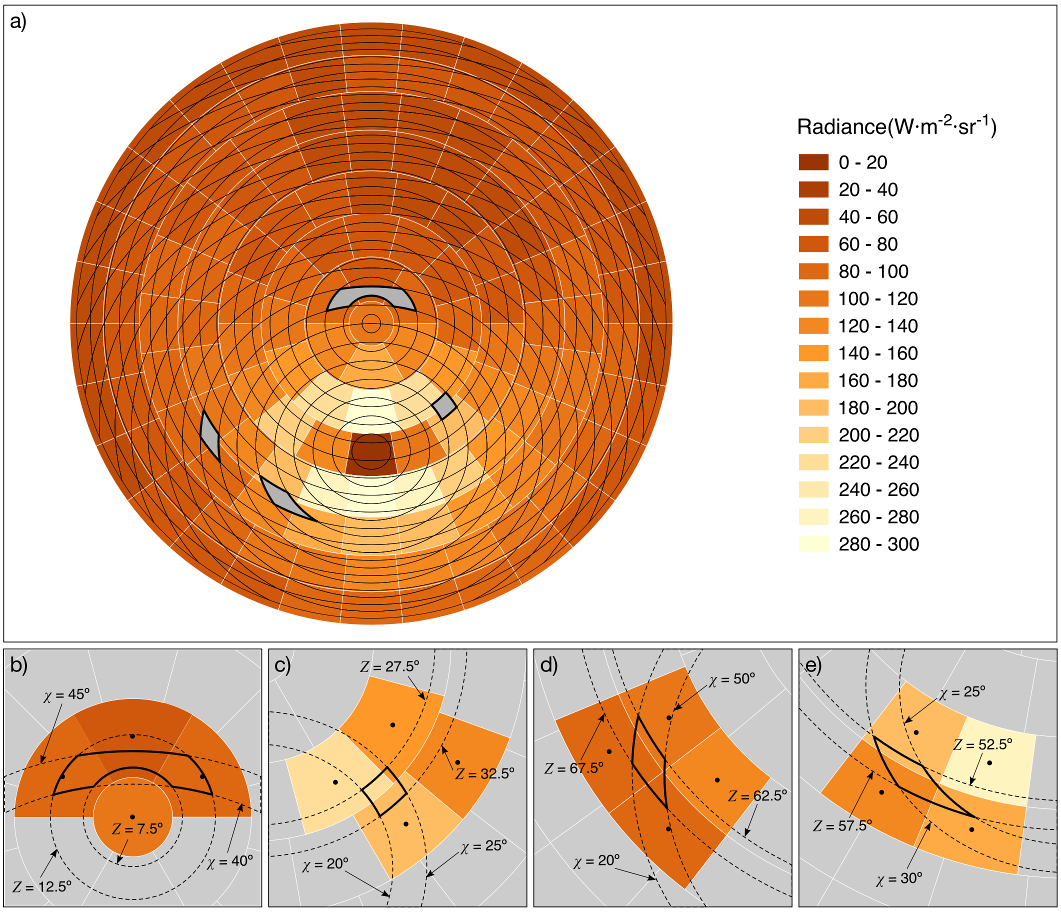

Fig. 9. Sky radiance distribution measured by a Sky Scanner EKO at Public University of Navarre station and EoSS's distribution (a). CIE sky patches involved in the radiance estimation of the four EoSS shaded in Fig. 9a (b-e).

The results obtained after the use of both procedures for the assignment of radiance/luminance to specific sky elements are shown in Table 1. As can be seen, the differences obtained for the four examples range between 5.27% and 9.59% (in absolute value). Regardless of the differences obtained, the application of both procedures reveals a series of advantages that the GIS-based method proposed in this paper presents as opposed to a spatial interpolation.

The most evident is the fact that, while applying a spatial interpolation, such as IDW, it is necessary to previously establish the number of sky patches to be considered (four in this example), the proposed procedure automatically selects the patches involved, i.e., only those covered by the EoSS in question. As can be seen in Fig. 9, it is a variable number of sky patches. Also, the GIS-based procedure eliminates the source of uncertainty involved in the selection of the IDW power parameter, or even the interpolation method to be used.

Finally, the aforementioned automatic selection derived from the use of the GIS-based method would lead to the fact that, when an EoSS is entirely within a single sky patch, it will take the radiance/luminance value of this patch. This is consistent with the assertion stated by Kobav et al. [22] that the value measured by a sky scanner represents the average value of luminance and radiance in the device FOV. However, if a spatial interpolation is applied, an interpolated value from the four closest patches will be assigned to the EoSS.

Table 1. Differences between the radiance values assigned to four EoSS by IDW interpolation and by the GIS-based procedure proposed.

EoSS	Z_e (º)	χ (º)	Sky patch	$\chi_{p\text{-}e}$ (º)	L_p ($W \cdot m^{-2} \cdot sr^{-1}$)	L_e GIS ($W \cdot m^{-2} \cdot sr^{-1}$)	L_e IDW ($W \cdot m^{-2} \cdot sr^{-1}$)	Dif. (%)
a)	(7.5-12.5)	(40-45)	1	11.09	89.97	85.48	89.90	5.27
			2	2.00	79.59			
			3	11.09	86.37			
			4	10.00	103.69			
b)	(27.5-32.5)	(20-25)	1	11.66	134.59	203.96	188.06	7.79
			2	6.06	192.08			
			3	7.93	232.46			
			4	10.25	143.76			
c)	(52.5-57.5)	(40-45)	1	9.91	97.46	102.90	108.88	-5.82
			2	6.46	95.24			
			3	7.96	119.85			
			4	10.58	139.16			
d)	(52.5-57.5)	(25-30)	1	11.01	175.52	155.99	170.95	-9.59
			2	5.74	129.37			
			3	7.47	198.55			
			4	11.48	266.90			

4. Conclusion

In this work, a GIS-based procedure has been proposed for the following:

1. The identification of the different spherical zones (EoSSs) obtained by combining the constant gradation (SSG) and constant indicatrix (SSS) spherical sectors.

2. The assignation of the radiance/luminance experimental values observed in the 145 routinely registered positions of the commercial sky scanners to each of the different EoSSs, corresponding to different solar elevations, whose geometry is different from that of the sky patches observed by such sky scanners.

The proposed procedure is easily adaptable to different configurations of sky patches measured by both commercial and experimental sky scanners. Therefore, other configurations, adapted for other purposes, could be considered by the described methodology. This methodology can be used for the development and calibration of radiance/luminance angular distribution models based on ground-based measurements and satellite-derived data.

Appendix A. Procedure for modeling the gradation and indicatrix functions

To model gradation or indicatrix functions from a series of routine radiance/luminance angular distribution measurements, a similar methodology can be followed independently for each.

Given that the aforementioned functions depend on the indicators used to characterize the different sky types under study, first intervals must be chosen in which the range of total variability for each of these indicators will be divided. For example, in Janjai et al. [17] and Janjai [18], the indicators are the solar zenith angle (Z_s) and the satellite-derived cloud index (n). Consequently, if the number of intervals chosen for the first one is p and for the second one q, there would be a $p \cdot q$ number of sky conditions or types to consider. Further, the angular amplitude of the SSSs and SSGs must also be decided initially. In this way, the SSGs can be defined for all subsequent analyses, but not the SSSs because these will depend on the Z_s.

Then, the angular distribution data observed experimentally should be treated with the goal of having a single angular distribution, averaged and referred to the solar meridian, for each of the $p \cdot q$ established sky conditions. This process involves the following stages:

a. Refer the 145 radiance/luminance measurements made by sky scanners at each moment to the corresponding solar meridian (see Fig. A.1). For this purpose, each patch measurement is rotated around the vertical direction, so that they are referenced to the solar meridian and not to the south at each moment, thus going from $L(Z,\gamma)$ to $L(Z,\gamma_{tosun})$. The results of this rotation constitute the database that will be used for the development and/or calibration of the model.

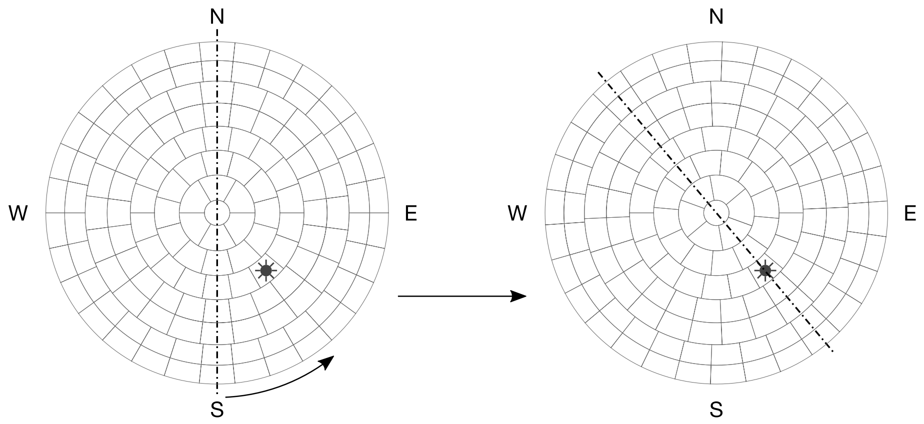

Fig. A.1. Rotation of the sky scanner measurements (referenced to the South) to referenced them to the solar meridian.

b. Group the angular distribution measurements prepared in the previous point, that belong to each of the $p \cdot q$ sky conditions. In this way $p \cdot q$ subgroups are obtained. Within each of them there will be an m variable number of registered angular distributions of radiance/luminance.

c. Average the m angular distributions within each of the $p \cdot q$ subgroups generated in the previous section. Thus, $p \cdot q$ average angular distributions of radiance/luminance are obtained (one for each subgroup). Each of them will have a certain Z_s and n.

The gradation function will include a series of coefficients depending on the sky conditions. Consequently, a recursive analysis of this function with respect to such conditions should be performed, as described below:

1. Set the value of one of the two indicators considered, for example n, and take the corresponding p angular distributions from the database, each with a different Z_s.
2. Follow the next steps for each of the p distributions derived in the previous stage:
   2.1. Define the SSSs corresponding to the Z_s of each of the p distributions contemplated, according to the angular amplitude chosen at the beginning of the process.

2.2. Determine the EoSSs corresponding to the intersections of the different SSGs and SSSs. For this step, the methodology proposed in the present work can be used.

2.3. Determine the radiance/luminance values corresponding to each of the EoSSs from the measured radiance/luminance values $L(Z,\gamma_{tosun})$ collected in the database. Again, the methodology proposed in the present study can be used for this purpose.

2.4. Identify the v EoSSs belonging to each of the successive SSSs and collect their values $L(Z_i,\chi)$, with i from 1 to v. It should be remembered that χ remains constant for each different SSS so that, for example, for the SSS corresponding to $\chi = \chi_1$, the relationships included in the Equation (A.1) can be established.

$$\frac{L(Z_1,\chi_1)}{L(0,Z_s)}=\frac{f(\chi_1)\cdot\varphi(Z_1)}{f(Z_s)\cdot\varphi(0)};\ \frac{L(Z_2,\chi_1)}{L(0,Z_s)}=\frac{f(\chi_1)\cdot\varphi(Z_2)}{f(Z_s)\cdot\varphi(0)};..........\frac{L(Z_v,\chi_1)}{L(0,Z_s)}=\frac{f(\chi_1)\cdot\varphi(Z_v)}{f(Z_s)\cdot\varphi(0)} \quad (A.1)$$

2.5. Divide each of the quotients obtained in the step 2.4 by any one taken as reference, whose position is given by the angle of zenith Z_{ref}. In this way, following the example of $\chi = \chi_1$, the equalities included in the Equation (A.2) are obtained.

$$\frac{\frac{L(Z_1,\chi_1)}{L(0,Z_s)}}{\frac{L(Z_{ref},\chi_1)}{L(0,Z_s)}}=\frac{\frac{f(\chi_1)\cdot\varphi(Z_1)}{f(Z_s)\cdot\varphi(0)}}{\frac{f(\chi_1)\cdot\varphi(Z_{ref})}{f(Z_s)\cdot\varphi(0)}};\ \frac{\frac{L(Z_2,\chi_1)}{L(0,Z_s)}}{\frac{L(Z_{ref},\chi_1)}{L(0,Z_s)}}=\frac{\frac{f(\chi_1)\cdot\varphi(Z_2)}{f(Z_s)\cdot\varphi(0)}}{\frac{f(\chi_1)\cdot\varphi(Z_{ref})}{f(Z_s)\cdot\varphi(0)}};......;1;.......;\frac{\frac{L(Z_v,\chi_1)}{L(0,Z_s)}}{\frac{L(Z_{ref},\chi_1)}{L(0,Z_s)}}=\frac{\frac{f(\chi_1)\cdot\varphi(Z_v)}{f(Z_s)\cdot\varphi(0)}}{\frac{f(\chi_1)\cdot\varphi(Z_{ref})}{f(Z_s)\cdot\varphi(0)}} \quad (A.2)$$

A simple algebraic manipulation of Equation (A.2) leads to Equation (A.3).

$$\frac{L(Z_1,\chi_1)}{L(Z_{ref},\chi_1)}=\frac{\varphi(Z_1)}{\varphi(Z_{ref})};\ \frac{L(Z_2,\chi_1)}{L(Z_{ref},\chi_1)}=\frac{\varphi(Z_2)}{\varphi(Z_{ref})};.....;1;....;\frac{L(Z_v,\chi_1)}{L(Z_{ref},\chi_1)}=\frac{\varphi(Z_v)}{\varphi(Z_{ref})} \quad (A.3)$$

The values of the first members of the equalities contained in the Equation (A.3) are known, because they are in the database built from the routine measurements, therefore, the points (Z_i , $\varphi(Z_i)/\ \varphi(Z_{ref})$) are also known as well as the curve that they define. If the process is repeated for $\chi = \chi_2$, $\chi = \chi_3$ … $\chi = \chi_s$, a family of curves will be obtained. According to Janjai et al. [17] and Janjai [18], these curves are similar and can be summarized in a single, final curve for each Z_s.

2.6. Determine the intersection point of the final curve obtained in step 2.5 with the vertical axis and consequently the value of $\varphi(0)/\varphi(Z_{ref})$.

2.7. Divide every quotient $\varphi(Z_i)/\varphi(Z_{ref})$ by $\varphi(0)/\varphi(Z_{ref})$, thus obtaining the series of values defined in Equation (A.4), which correspond to the values of the relative gradation function corresponding to the Z_s considered.

$$\frac{\frac{\varphi(Z_1)}{\varphi(Z_{ref})}}{\frac{\varphi(0)}{\varphi(Z_{ref})}} = \frac{\varphi(Z_1)}{\varphi(0)}\ ;\ \frac{\frac{\varphi(Z_2)}{\varphi(Z_{ref})}}{\frac{\varphi(0)}{\varphi(Z_{ref})}} = \frac{\varphi(Z_2)}{\varphi(0)}\ ;\ \ldots\ldots\ldots \frac{\frac{\varphi(Z_v)}{\varphi(Z_{ref})}}{\frac{\varphi(0)}{\varphi(Z_{ref})}} = \frac{\varphi(Z_v)}{\varphi(0)} \qquad \text{(A.4)}$$

By repeating the full procedure included in step 2 of the procedure for the p different Z_s and, subsequently, doing the same for the q possible n, all the necessary data will be available to adjust the relative gradation function model.

The process would be analogous for the indicatrix function. The difference is that, in this case, it would consider the different SSGs, in which the gradation function remains constant. Again, the methodology proposed in this paper would be necessary to complete the different steps of the aforementioned process.

Acknowledgments

This work was performed in the framework of Project IRILURREFLEX (ENE2017-86974-R), financed by the Spanish State Research Agency (Agencia Estatal de Investigación, AEI) and European Regional Development Fund (Fondo Europeo de Desarrollo Regional, FEDER). The authors would like to thank the anonymous reviewers for their useful comments that greatly improved this paper. They also thank the Public University of Navarre for awarding Ignacio García Ruiz a Doctoral Fellowship.

References

[1] B. Mayer, A. Kylling, Technical note: The libRadtran software package for radiative transfer calculations - description and examples of use, Atmos. Chem. Phys. 5 (2005) 1855–1877. doi:10.5194/acp-5-1855-2005.

[2] M. Kocifaj, Unified model of radiance patterns under arbitrary sky conditions, Sol. Energy. 115 (2015) 40–51. doi:10.1016/j.solener.2015.02.019.

[3] P. Moon, D.E. Spencer, Illumination from a non-uniform sky, Trans. Illum. Eng. Soc. 37 (1942) 707–726.

[4] R. Kittler, Standardisation of outdoor conditions for the calculation of daylight factor with clear skies, in: Proc. CIE Intersessional Conf. Sunlight Build., Newcastle upon Tyne, 1965: pp. 273–285.

[5] CIE, Natural Daylight. Official Recommendation, 1955.

[6] CIE, Standardization of luminance distribution on clear skies, 1973.

[7] M. Perraudeau, Luminance models, in: Natl. Light. Conf. Daylighting Colloq., Cambridge, UK, 1988: pp. 291–292.

[8] K. Matsuura, T. Iwata, A model of daylight source for the daylight illuminance calculations on the all weather conditions, in: Proc. 3rd Int. Daylighting Conf., Moscow, Russia, 1990.

[9] R. Perez, P. Ineichen, R. Seals, J.J. Michalsky, R. Stewart, Modeling daylight availability and irradiance components from direct and global irradiance, Sol. Energy. 44 (1990) 271–289. doi:10.1016/0038-092X(90)90055-H.

[10] A.P. Brunger, F.C. Hooper, Anisotropic sky radiance model based on narrow field of view measurements of shortwave radiance, Sol. Energy. 51 (1993) 53–

64. doi:10.1016/0038-092X(93)90042-M.

[11] R. Perez, R. Seals, J.J. Michalsky, All-weather model for sky luminance distribution—Preliminary configuration and validation, Sol. Energy. 50 (1993) 235–245. doi:10.1016/0038-092X(93)90017-I.

[12] N. Igawa, Y. Koga, T. Matsuzawa, H. Nakamura, Models of sky radiance distribution and sky luminance distribution, Sol. Energy. 77 (2004) 137–157. doi:10.1016/j.solener.2004.04.016.

[13] N. Igawa, Improving the All Sky Model for the luminance and radiance distributions of the sky, Sol. Energy. 105 (2014) 354–372. doi:10.1016/j.solener.2014.03.020.

[14] CIE, Spatial Distribution of Daylight – CIE Standard General Sky, 2003.

[15] M. Kocifaj, L. Kómar, F. Kundracik, PePSS - A portable sky scanner for measuring extremely low night-sky brightness, J. Quant. Spectrosc. Radiat. Transf. 210 (2018) 74–81. doi:10.1016/J.JQSRT.2018.02.017.

[16] CIE, Guide to recommended practice of daylight measurement, Vienna, Austria, 1994.

[17] S. Janjai, I. Masiri, M. Nunez, J. Laksanaboonsong, Modeling sky luminance using satellite data to classify sky conditions, Build. Environ. 43 (2008) 2059–2073. doi:10.1016/j.buildenv.2007.12.009.

[18] S. Janjai, A Satellite-Based Sky Luminance Model for the Tropics, Int. J. Photoenergy. 2013 (2013) 1–11. doi:10.1155/2013/260319.

[19] L. Kómar, A. Rusnák, R. Dubnička, Analysis of diffuse irradiance from two parts of sky vault divided by solar meridian using portable spectral sky-scanner, Sol. Energy. 96 (2013) 1–9. doi:10.1016/J.SOLENER.2013.07.003.

[20] J.L. Torres, M. de Blas, A. García, A.M. Gracia, A. de Francisco, Sky luminance

distribution in the North of Iberian Peninsula during winter, J. Atmos. Solar-Terrestrial Phys. 72 (2010) 1147–1154. doi:10.1016/j.jastp.2010.07.001.

[21] J.L. Torres, M. de Blas, A. García, A.M. Gracia, A. de Francisco, Sky luminance distribution in Pamplona (Spain) during the summer period, J. Atmos. Solar-Terrestrial Phys. 72 (2010) 382–388. doi:10.1016/j.jastp.2009.12.005.

[22] M.B. Kobav, G. Bizjak, D. Dumortier, Characterization of sky scanner measurements based on CIE and ISO standard CIE S 011/2003, Light. Res. Technol. 45 (2012) 504–512. doi:10.1177/1477153512458916.